Optical Lithography Simulation and Photoresist Optimization for Photomask Fabrication

Benjamen M. Rathsack[1], Cyrus E. Tabery[1], Steven A. Scheer[1], Mike Pochkowski[2], Cece Philbin[3], Franklin Kalk[3], Clifford L. Henderson[4], Peter D. Buck[5] and C. Grant Willson[1]

[1]Department of Chemical Engineering, The University of Texas at Austin, Austin, TX 78712

[2] ETEC Systems Inc., 9100 S. W. Gemini Dr., Beaverton, OR 97008
[3] DPI Reticle Technology Center LLC, 2011 Greenhill Dr., Round Rock, TX 78664
[4] Georgia Institute of Technology, 7778 Atlantic Dr., Atlanta, GA 30332
[5] Dupont Photomask Inc., 1955 NE Division St. Gresham, OR 97030

ABSTRACT

The demand for smaller and more uniform features on photomasks is rapidly increasing. The complexity of these patterns is also increasing with the need for optical proximity correction and phase shifting structures. These complex mask features demand unprecedented accuracy in pattern placement and dimensional control. We have conducted research designed to optimize the process for laser pattern generation by improving resolution and process latitude. Lithographic simulation was utilized for process optimization because of the very high cost of mask patterning and metrology experiments.

Benchmark resist characterization and simulations were performed on IP3600 (TOK), which is a resist commonly used in photomask fabrication. High resolution I-line resists provided by Sumitomo (PFI88A5), Shipley (i120, SPR1055), Clariant (AZ7905) and Olin (RX620, RX672) were characterized and simulated to explore the potential of high-contrast (notch) I-line resists for photomask fabrication. These materials were characterized on AR3 chromium oxide coated quartz substrates. The Dill exposure (*A*, *B* and *C*) and development (*R(m)*) parameters were extracted using custom hardware and software. A custom hotplate was constructed that provides a post-application bake profile that mimics that of a production photomask bake process. The resists were compared by simulating their process windows using pattern generator aerial images supplied by ETEC Systems Inc. The simulations predicted that the implementation of a post exposure-bake, higher exposure dose and longer development time with diluted developer would provide dramatic improvements in resolution and linewidth uniformity without significantly lowering production rates. This paper describes modeling parameters and simulations for the current benchmark resist IP3600 and one high-resolution resist (PFI88A5) to demonstrate the principles used to optimize laser photomask lithography. The modeling parameters for the other resists were provided to each respective vendor.

The predictions derived from the simulations were tested at the DPI Reticle Technology Center using an ETEC ALTA 3500 pattern generator. The linewidth and sidewall profiles of the test plates were measured, and the results confirm the predicted increase in process latitude for linewidths as small as 0.3 μm. Lithography simulation is clearly a valuable tool for optimizing the laser photomask fabrication process.

Keywords: photomask, photoresist, lithography simulation

1. INTRODUCTION

The fabrication of photomasks with smaller and more uniform linewidths is critical for the development of phase-shifting and optical proximity correction features. The reticle has been identified as a large contributor of CD error in 0.25 μm DUV lithography [1]. The extension of DUV lithography through implementation of resolution enhancements like phase shifting and OPC requires further reduction in the mask critical-dimension error [2]. Optimization of the laser pattern generator process can reduce photomask CD error and improve resolution. Lithography simulation and mask fabrication trials have been utilized to widen the process latitude and improve linewidth control for resist features down to 0.3 μm on production laser pattern generators.

[1] Correspondence: Email: willson@che.utexas.edu; http://willson.cm.utexas.edu/

Significant improvements have been made in I-line resists over the last several years. Very high-contrast resists have been formulated through a variety of resist formulation approaches: 1) the “tandem approach”, which utilizes bi-modal novolak molecular-weight distributions and dissolution rate enhancers [3]; 2) low-polydispersity, highly inhibiting, non-fractionated novolaks with large inhibiting PACs (photoactive compound) and smaller co-PACs [4]; 3) highly branched novolaks with controlled end groups that take advantage of the *ortho-ortho* linkage effects on dissolution inhibition [5,6]. Our goal was to determine the extent to which the high-performance I-line resist chemistry developed for IC manufacturing could be utilized to improve laser photomask fabrication.

Lithography simulation was used to optimize the development, post-application bake and post-exposure bake conditions for I-line resists on photomasks. I-line resists have been characterized by extracting exposure (*A*, *B* and *C*) and development rate (*R(m)*) parameters. The exposure and development rate parameters were extracted from experiments on AR3 coated photomask substrates. The *R(m)* functions of the high resolution I-line resists contain a "notch" in the dissolution rate function. Lithography simulations of photomask resist profiles using these *R(m)* functions show that higher resolution and wider process latitude can be achieved through the use of lower developer concentrations, longer development times and higher exposure doses combined with a post-exposure bake. The combination of lower developer concentration and longer development time increases the sidewall angle and minimizes the linewidth sensitivity to dose. The post-exposure bake is required to remove the standing waves that are exaggerated in the high contrast resists. The removal of standing waves in the resist reduces the linewidth variation in the resist profile and removes undissolved resist close to the photomask surface, which is referred to as “scumming.” Manufacturing trials at the Reticle Technology Center (DPI) confirm the simulated resolution and focus-exposure latitude improvements for resist structures down to 0.3 μm.

2. THEORY

2.1 Resist and Photomask Index of Refraction Measurements

R(m) function determination requires knowledge of the index of refraction of both the resist and substrate. Photomask substrates are coated with a graded chromium oxide, chromium and silicon dioxide film stack as shown in Figure 1.

Chromium Oxide	35 nm
Chromium	70 nm
Silicon Dioxide	6.35 mm

Figure 1: Photomask Film Stack

The index of refraction of the chromium oxide layer varies due to an oxide concentration gradient through the thickness of the film. An ellipsometer was used to determine the index of refraction of the substrate as a function of wavelength. The polarization change needs to be measured from light reflected perpendicular to the substrate surface for optical thin film thickness calculations. An ellipsometer is not capable of making polarization measurements perpendicular to the substrate. Hence, the composite index of refraction of the substrate was determined from the additive effects of the individual index of refraction values in each layer of the film stack. The index of refraction of chromium and silicon dioxide (homogeneous layers) has been previously measured. The index of refraction of the chromium oxide layer was extracted from the model by knowing the total polarization change through the substrate and the polarization effects of the previously characterized layers. The composite index of refraction of the photomask substrate was then calculated by summing the effects of the index of refraction in each layer of the film stack.

2.2 Film Thickness Calculations on Photomask Substrates

Thickness measurements of resist films were made by the analysis of the constructive and destructive interference patterns in reflected light from the film stack as a function of wavelength. Accurate measurements on mask substrates requires knowledge of the real and complex index of refraction of both the resist and the substrate, because the substrate absorbs light in the analysis wavelength range of 500 to 900 nm. Equation 1 was used to calculate film thickness from the measured maxima and minima in the reflectivity as a function of wavelength [7]

$$d = \frac{(fp + \arctan(\frac{2n_1k_2}{n_1 - n_2 - k_2})) \times l}{4pn_1} \qquad (1)$$

where d is the film thickness, f is the fringe order, n_1 is the real index of refraction of the photoresist, n_2 is the real index of refraction of the mask substrate, k_2 is the complex index of refraction of the substrate and l is the wavelength of the light. The calculation includes the absorption of light (k_2) by the photomask substrate. The measurement of film thickness on mask substrates has been included into the capabilities of our multi-wavelength development rate monitor (DRM) [8].

2.3 Resist Exposure Model Parameters

I-line resist modeling requires measurements of the exposure and reaction parameters A, B and C first described by Dill and co-workers [9]. Our laboratory has established rigorous methods for extracting A, B and C parameters that take into account the change in the index of refraction of the resist [10]. Exposure parameter extraction was accomplished using software developed at The University of Texas at Austin as described in previous papers [11,12].

2.4 Development Rate Model Parameters

Resist modeling also requires the measurement of the dissolution rate as a function of film thickness and dose. These data are then fit to one of several dissolution rate models that have been developed to support lithography simulators. The Enhanced Mack model describes both the enhancement of the dissolution rate by exposed PAC and the inhibition of the rate by the unexposed PAC [13]. Modern high-resolution I-line photoresists have a "notch" behavior characterized by a sharp increase in development rate at a critical normalized photoactive-compound concentration. New development rate models have been constructed to account for this notch behavior. A comparison of notch models reveals that the Dammel model [3] and Notch model [14] provide the best overall fit to experimental dissolution rate data collected for multiple resists [15]. The Notch model was chosen over the Dammel model for high resolution I-line resist modeling, since it is available in a commercial simulation package. The Enhanced Mack and Notch development rate models were used to establish a semi-empirical relationship between the development rate and the relative PAC concentration.

2.5 Photomask Resist Process Window Optimization

The process window for printing resist features on photomask substrates can be maximized through “line-edge optimization”. The exposure image and resist dissolution response is evaluated at the bottom of the nominal feature edge. The optimal resist response occurs when the resist completely dissolves with perpendicular sidewalls while maintaining the nominal linewidth.

The relative PAC concentration (m) can be calculated in any volume element in the film. The m is calculated by convolving the aerial image and the resist exposure parameters. A change in PAC concentration through the horizontal position in the resist defines a relative PAC gradient (*Ñm*) at the nominal feature edge. An optimal exposure dose exists that maximizes *Ñm* at the nominal resist feature edge. The optimum process latitude is achieved when the maximum *Ñm* and the maximum resist contrast (g_R) occur at the same relative PAC concentration ($m*$), and that concentration is located at the edge of the resist feature ($x*$) where R is the dissolution rate of the resist and x is the horizontal direction parallel to the substrate. (Equations 2 and 3).

$$\left.\frac{\partial R}{\partial x}\right|_{x*} = g_R \frac{\partial m}{\partial x} \qquad \nabla m = \frac{\partial m}{\partial x} \qquad (2)$$

$$g_R\left(m^*\right) = \frac{dR}{dm} \qquad (3)$$

The resist contrast is maximized at $x*$ by changing the developer concentration. A consequence of maximizing the contrast of a resist is the amplification of standing waves in the resist. Therefore, a post-exposure bake has been introduced to diffuse the PAC and reduce standing waves.

3. EXPERIMENTAL

3.1 Photoresist Coating, Post Application Bake and Exposure Conditions

Two photoresists, IP3600 (TOK) and PFI88A5 (Sumitomo), were spin-coated at a thickness of 570 nm on 4 in. diameter by 0.02 in. thick AR3 coated quartz disks from Hoya Corp. using a PWM32 Headway spinner. A hotplate was built that mimics the post-application bake temperature-time profile of the surface of a mask blank subject to the PAB cycle at a commercial coating facility. The hotplate incorporates a gain scheduled temperature control system that heats the thinner substrate surface to a temperature vs. time profile that matches that of the thicker commercial substrate. The system can control the surface temperature of the center of the substrate to within $\pm$ 1 °C of the programmed bake profile based on measurements made with a Thermal Map 2 (Sensarray). The PAB trajectory is shown in Figure 2. The divergence in the cooling temperature between the processes is not expected to interfere with the resist response since the solvent concentration in the film should not change at the lower bake temperatures [16,17]. The coated photoresist films were exposed with an Oriel 200 W Mercury arc lamp at a wavelength of 365 nm.

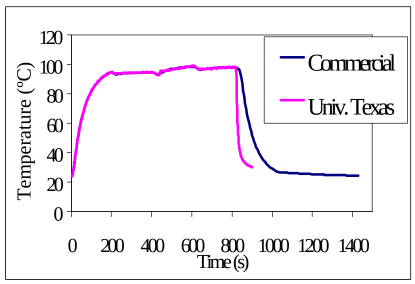

Figure 2: Photomask Post-Application Bake Temperature Profiles

3.2 Index of Refraction Measurements for Photomask Resists and Substrate

The index of refraction of IP3600 and PFI88A5 was measured using a J. A. Woollam Co. Variable Angle Spectroscopic Ellipsometer (VASE ®) system with WVASE software version 2.92. The index of refraction was measured between 300 nm and 1000 nm for both exposed (E) and unexposed (UE) resists on silicon substrates. The Cauchy coefficients presented in Table 1 allow calculation of the index of refraction values of each resist at any wavelength between 500 nm and 900 nm. The index of refraction was also measured at the exposure wavelength of 365 nm.

Table 1: Resist Index of Refraction Measurements (Cauchy Coefficients)

Resist	**A**	**B (μm^2)**	**C (μm^4)**	**n at 365nm**	**k at 365nm**
IP3600-UE	1.6114	0.0046	0.0020	1.6947	0.0257
IP3600-E	1.5917	0.0102	0.0004	1.6887	0.0031
PFI88A5-UE	1.6024	0.0095	0.0009	1.7006	0.0211
PFI88A5-E	1.5908	0.0108	0.0001	1.6863	0.0010

The Cauchy coefficients are used in the DRM and static thickness analysis tools to measure film thickness. The index of refraction data are also used to model the standing waves that occur on mask substrates.

The real and complex parts of the index of refraction of a round AR3 coated Hoya mask substrate were measured by J. A. Woollam to be 1.63 and 0.28 at 365 nm, respectively. These values for a 6×6 in.^{2} Hoya production mask were measured to be 1.38 and 0.44, respectively. The index of refraction of photomask substrates can vary from sample to sample depending on the variation in chromium oxide thickness in the AR3 coatings. The index of refraction must be carefully measured in order to do precise simulation.

3.3 Exposure Parameter Extraction (*ABC*)

ABC values were extracted by measuring the transmittance of samples at 365 nm as a function of exposure dose. The resists were coated at a film thickness of 570 nm on transparent quartz substrates that were made by etching the chromium layer from the round Hoya substrates. The modified Hoya substrates were used for the *ABC* experiments so that the time dependent PAB would replicate the PAB used for resists studied in DRM and ellipsometry experiments. The resists were baked for 815 seconds with the mask PAB profile (Figure 2). The *ABC* values for the resists are shown in Table 2.

Table 2: ABC Exposure Parameters

Resist	**A (μm^{-1})**	**B (μm^{-1})**	**C (cm^2/mJ)**
IP3600	0.8607	0.1074	0.0142
PFI88A5	0.7044	0.0400	0.0105

How accurate are the *ABC* values? The absorption coefficient of the resist is related to the complex index of refraction of the resist at the exposure wavelength. The complex index of refraction can be calculated from the *A* and *B* values at the exposure wavelength ($k_{unexposed} = l(A+B)/(4p)$) which can be compared to the complex index of refraction measured by ellipsometry. The complex index of refraction calculated from the *A* and *B* values is very close to the values measured with an ellipsometer (IP3600: k_{AB} is 0.028 and k_{ELL} is 0.026; PFI88A5: k_{AB} is 0.021 and k_{ELL} is 0.021). The close correlation increases our confidence in the *A* and *B* values.

3.4 Simulated Swing Curves for Photomask Resists

The reflectivity swing curves for resists are the result of the interference of transmitted and reflected light at the air-resist and resist-substrate interfaces. The propagation of light through the resist depends on the index of refraction of the photomask substrate, the index of refraction of the resist (*k* is calculated from Dill's *A* and *B* parameters) and the intensity of light exposing the resist. The swing curves of IP3600 and PFI88A5 were simulated (PROLITH/2 6.04) to check on the accuracy of the measurements of the index of refraction of the resist and substrate. The simulated swing curves are very close to the swing curves measured by Hoya [18]. The simulated swing curves have reflectivity minima at film thickness around 445 nm and 555 nm that are close to the commercially measured minima at 460 nm and 570 nm (Figure 3). The optical constants for the resist and substrate appear to be sufficiently accurate for further simulation.

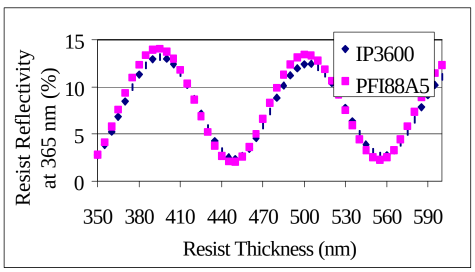

Figure 3: Simulated Swing Curves for IP3600 and PFI88A5

3.5 Standing Waves in Resists on Photomask Substrates

Standing waves cause a periodic variation in *m* as a function of thickness in the resist. Unlike most silicon wafer I-line processes, the current laser photomask writing process does not use a post-exposure bake to diffuse the PAC and remove the standing waves. Development rate measurements reveal that standing waves exist in resists on photomask substrates in spite of the antireflective AR3 coating. Reducing the developer concentration increases the resist contrast and exaggerates the effects of standing waves in the resist. The oscillations in dissolution rate versus resist thickness for IP3600 with 0.20N TMAH (NMD-W) at a 115 mJ/cm^2 dose are evident in Figure 4. The dissolution rate approaches zero at the destructive interference nodes.

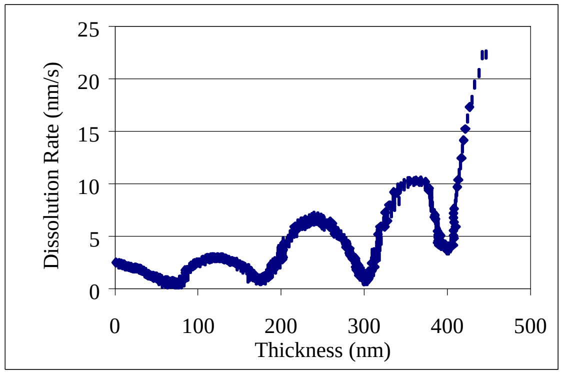

Figure 4: DRM Measurements for IP3600 Showing Standing Waves

3.6 Post-Exposure Bake for Laser Photomask Resists

DRM experiments showed that development of IP3600 and PFI88A5 with 0.26N TMAH (NMD-W) requires a PEB at a steady-state temperature of 114 °C for a minimum of 90 s to remove standing waves. The PEB temperature is higher than the normal 110 °C PEB that is recommended for I-line photoresists. It is hypothesized that the 815 s PAB has depleted more of the resist solvent and thus increased the glass transition temperature of the resist. We set the PEB temperature to be 120 °C at the surface of the mask to insure that the PAC would diffuse. A Thermal Map 2 (Sensarray) device was used to measure the surface temperature profile of the mask on a commercial production bake plate set at a 128 °C. Our hotplate control system was programmed to mimic this PEB temperature profile measured on the surface of the commercial mask. The programmed bake maintains a steady-state minimum temperature above 114 °C for 90 s. The post-exposure bake temperature profile of a commercial photomask hotplate was used as a set point trajectory for our programmable hotplate (Figure 5).

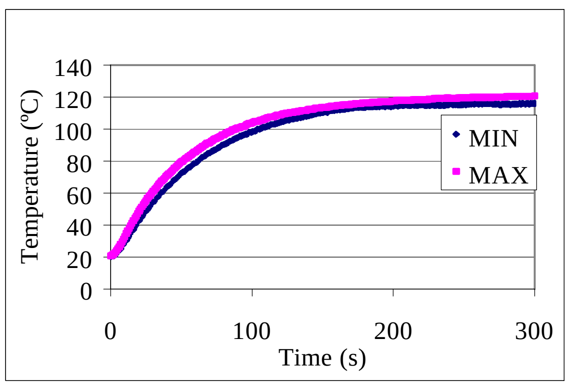

Figure 5: Photomask Post-Exposure Bake Temperature Profile

3.7 *R(m)* Development Rate Models as a Function of Developer Concentration

R(m) functions were measured for IP3600 and a group of high-resolution I-line resists supplied by Sumitomo, Clariant, Shipley and Olin using the photomask PAB and PEB profiles in Figures 2 and 5. The *R(m)* curves for all the resists developed with 0.26 N TMAH (vendor recommended developer) show a wide range of dissolution rate responses. The data for IP3600 were fit using the Enhanced Mack model, and the other data were fit using the Notch model (Figure 6). We have measured the *A*, *B*, *C* and *R(m)* parameters for all of the supplied resists and transmitted the parameters to the respective vendors. To date, we have only studied IP3600 and PFI88A in detail.

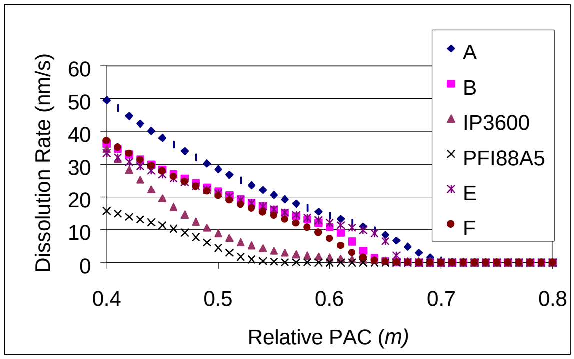

Figure 6: *R(m)* Curves for Various I-line Resists

All of the resists have a distinct dissolution rate notch except for IP3600. The notches in resists A, B, E and F are evident at *m* concentrations greater than 0.6, which indicates formulation for low-dose responses or high sensitivity. Low exposure doses and fast development rates (high throughput) are optimum for lithography on silicon. Photomask lithography throughput is limited more by raster write time (hours) than exposure dose and development time. Line edge optimization shows that the dissolution rate notch of the resists needs to occur at m^* where the $\tilde{N}m$ is maximized. Simulation (PROLITH2/ 6.04) reveals that the $\tilde{N}m$ is maximized for IP3600 and PFI88A5 at exposure doses of 210 mJ/cm^2 and 260 mJ/cm^2, respectively (Figure 7). Corresponding simulations of the *m* concentration at the line edge reveals that m^* is 0.3 for IP3600 at the optimum dose of 210 mJ/cm^2 (Figure 8). PFI88A5 also has a maximum $\tilde{N}m$ at a m^* of 0.3. The dissolution rate notch of the resist needs to be located at or near a m* of 0.3 to optimize resolution. Therefore, we chose to focus on the photomask benchmark resist IP3600 and PFI88A that have dissolution rate notches at a *m* closest to the optimal m^* of 0.3.

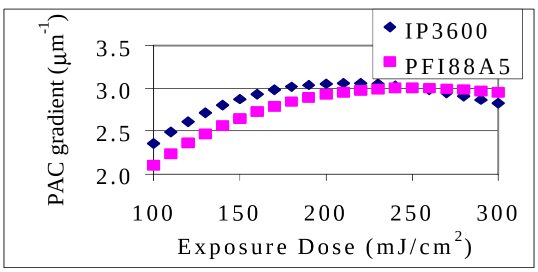

Figure 7: Optimum Exposure Dose to Maximize $\tilde{N}m$ at the Edge of the Resist Feature

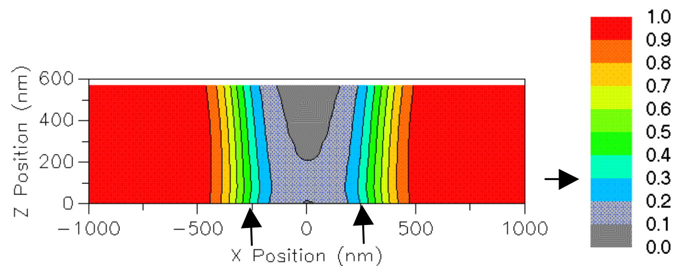

Figure 8:PAC Distribution: Maximum $\tilde{N}m$ at the line edge occurs at an m* of 0.3 for IP3600 (210 mJ/cm^2)

The location of the notch of each of the resists can be moved closer to the location of the optimum PAC gradient through the use of lower developer concentration. *R(m)* functions were extracted from IP3600 and PFI88A5 films developed with several developer concentrations (NMD-W) shown in Figures 9 and 10, respectively.

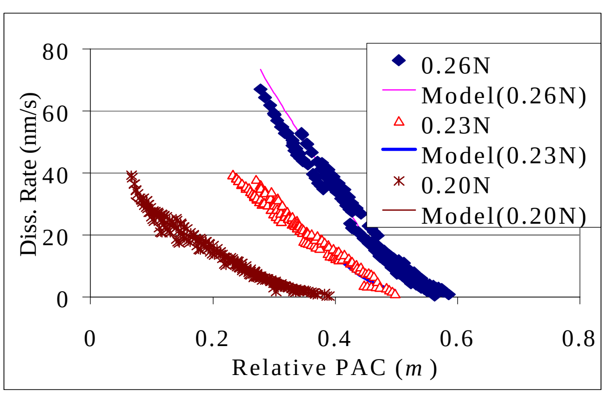

Figure 9: *R(m)* Functions for IP3600 Developed with 3 Developer Concentrations

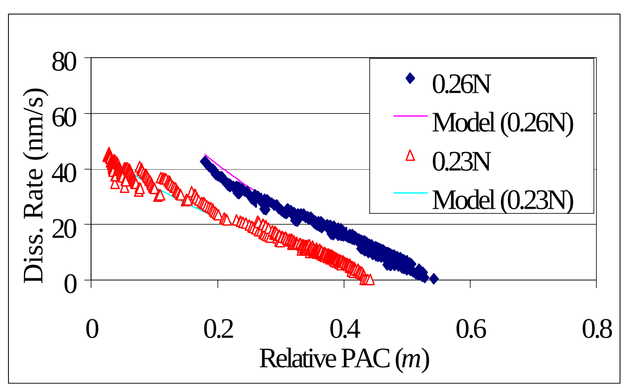

Figure 10: *R(m)* Functions for PFI88A5 Developed with 2 Developer Concentrations

PFI88A5 shows a larger development notch than IP3600 in the *R(m)* data for both 0.26N TMAH and 0.23N TMAH. The sharp notch indicates a high theoretical contrast that should result in a steeper sidewall angle and ultimately an increase in the focus-exposure process latitude over IP3600. Lower developer concentration shifts the development rate response to higher doses (lower *m*). The optimum developer concentration was chosen to place the dissolution rate notch at a m^* of 0.3 where the $\tilde{N}m$ is maximum.

3.8 Simulated Standing Waves in IP3600 without a PEB

Simulation (PROLITH/2 6.04) of a 0.5 µm isolated space exposed in IP3600 with an 80 mJ/cm^2 dose and developed with 0.26N TMAH developer concentration reveals standing waves. The simulated resist profile has 5 low dose nodes (standing waves) where the development is very slow (Figure 11). The standing waves produce scumming, poor sidewall angles and poor CD sensitivity to dose. Simulation of IP3600 resist profiles using a post-exposure bake with an estimated 50 nm diffusion length reduces the standing waves (Figure 12). The reduction of standing waves is predicted to reduce scumming and improve the focus-exposure process window.

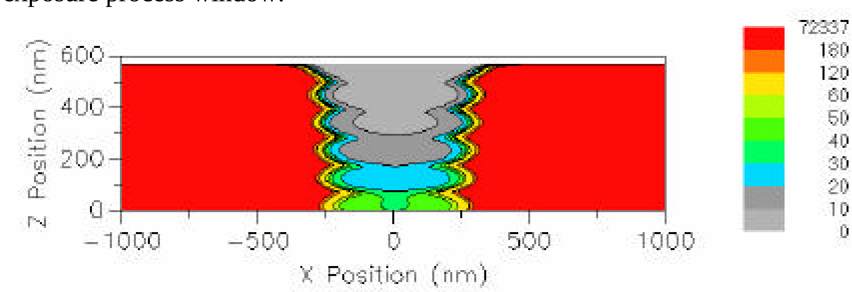

Figure 11: Simulated IP3600 Isolated Resist Space Developed over Time (s) without a PEB

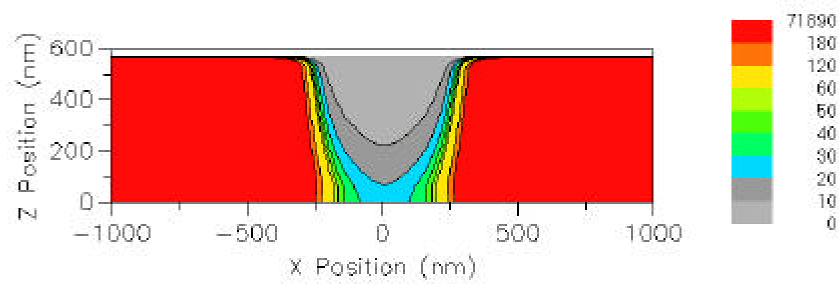

Figure 12: Simulated IP3600 isolated resist space developed over time (s) with a PEB

Manufacturing trials at DPI Reticle Technology Center (RTC) confirmed that the post-exposure bake process removes standing waves in IP3600. Focus-exposure (9 × 9) test patterns were exposed in IP3600 and developed with 0.23N TMAH (TOK brand developer: NMD-W) for 90 s with and without PEB. An inspection SEM (JEOL JWS-7815) was used to make linewidth measurements and examine the resist profiles. The resist profiles of 0.5 µm isolated spaces at the best dose (110 mJ/cm^2) reveal that the post-exposure bake removed the scumming throughout focus (Figure 13). The resist scumming is due to undeveloped resist located in the region of low dose of the standing wave. Close inspection of "X-features" at best focus reveals that the sidewall variations due to standing waves are removed by the post-exposure bake. The use of a post-exposure bake for photomask fabrication at RTC confirmed the predictions of the simulations and improved the focus-exposure process latitude.

Focus: -0.4 µm/ No PEB

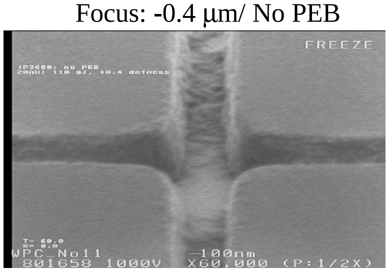

Focus: 0 µm/ No PEB

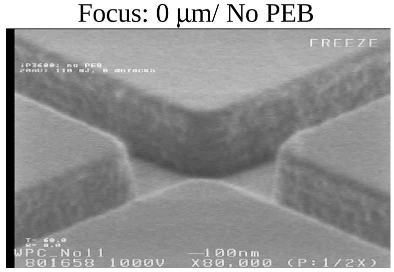

Focus: +0.4 µm/ No PEB

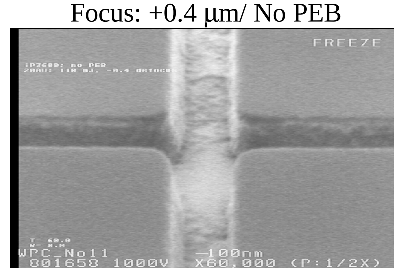

Focus: -0.4 µm/ PEB | Focus: 0 µm/ PEB | Focus: +0.4 µm/ PEB

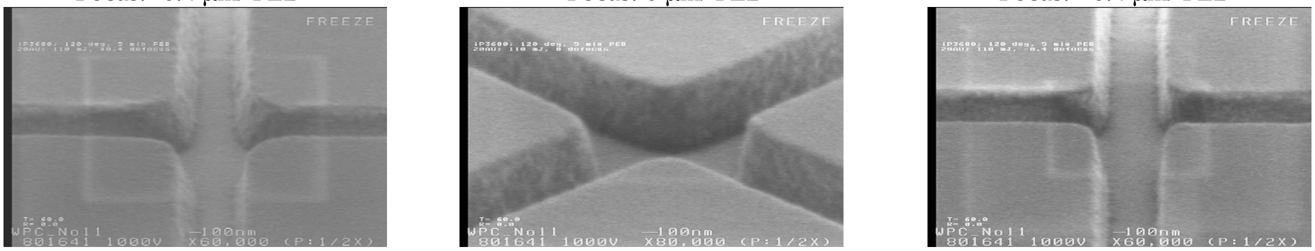

Figure 13: Photomask Post-Exposure Bake Improves Focus-Exposure Process Latitude (IP3600)

3.9 Process Window Simulations for IP3600 and PFI88A5

The SEM pictures reveal that the current photomask process using optical pattern generators without a post-exposure bake has a limited process window below 0.5 µm. Simulations of 0.5 µm IP3600 (isolated spaces) resist profiles developed with a 0.20N TMAH developer concentration reveal a larger exposure dose-development time process window than profiles developed with 0.26N TMAH (Figure 14 and 15). The simulated process window has highlighted the isolated resist features that have a 82°+ sidewall angle and a ± 5% linewidth latitude for a 0.5 µm optical pattern generator aerial image. The lower developer concentration, higher exposure doses and longer development times result in better sidewall angles and less linewidth sensitivity to dose, which produces a larger process window. Lower developer concentration should also minimize resist loss in the unexposed regions.

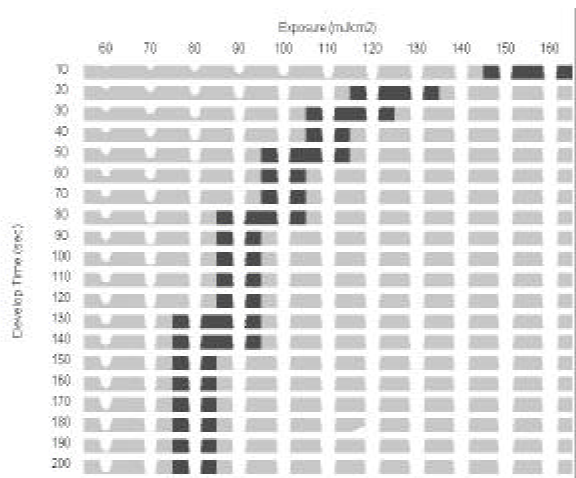

Figure 14: IP3600/ 0.26N TMAH/ No PEB

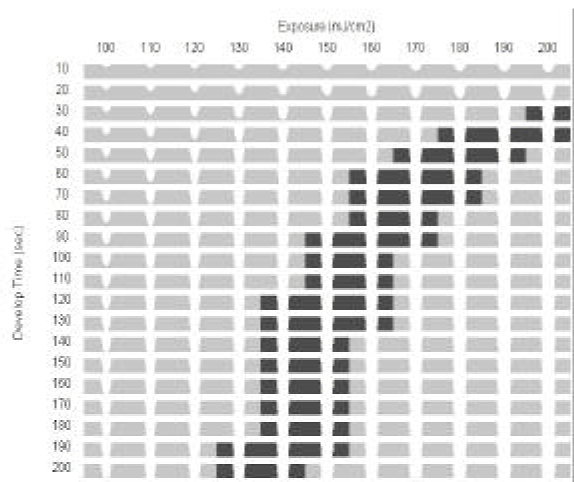

Figure 15: IP3600/ 0.20N TMAH/ PEB

Simulation of 0.5 µm PFI88A5 (isolated spaces) resist profiles developed with a 0.26N TMAH developer concentration reveals a larger process window than IP3600 (Figures 16 and 17). The increase in the PFI88A5 process window is due to the higher theoretical contrast produced from the notch in the *R(m)* function and larger $\tilde{N}m$ at higher exposure dose. Simulations of the PFI88A5 developed using a lower developer concentration of 0.23N TMAH further increased the exposure-development process latitude.

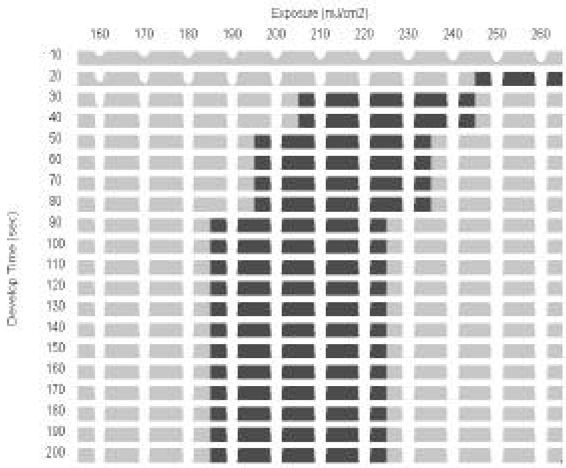

Figure 16: PFI88A5/ 0.26N TMAH/ PEB

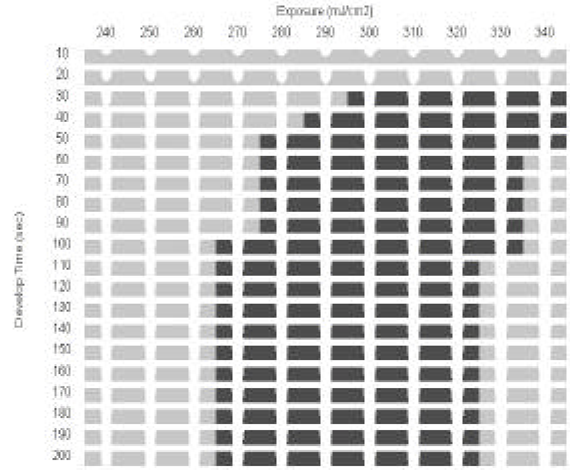

Figure 17: PFI88A5/ 0.23N TMAH/ PEB

Manufacturing trials at DPI (RTC) confirmed the simulated process latitude results for each resist. IP3600 (0.20 N TMAH/ 180 s dev./ PEB) and PFI88A5 (0.26N TMAH/ 180 s dev./ PEB) both showed dramatic focus-exposure process latitude improvements over IP3600 (0.26N TMAH/ 60 s dev./ No PEB) for 0.5 and 0.3 µm features. IP3600 (0.26N TMAH/ no PEB) is scummed even at best focus for a 0.3 µm isolated space. PFI88A5 (0.26N TMAH/ PEB) revealed the highest resolution with a clear 0.25 µm isolated space at best focus. A summary of the Bossung plots of IP3600 and PFI88A5 are in Table 3 (Figures 18-23). SEM pictures of isolated spaces for IP3600 and PFI88A5 are in Figures 24-29.

Table 3: Focus-Exposure Process Latitude Improvements for IP3600 and PFI88A5

	IP3600 0.5 µm (0.26N/ No PEB)	**IP3600 0.5 µm (0.20N/ PEB)**	**PFI88A 0.5 µm (0.26N/ PEB)**	**IP3600 0.3 µm (0.20N/ PEB)**	**PFI88A 0.3µm (0.26N/ PEB)**
Dose to Size (mJ/cm^2)	95	135	205	142	210
Exp Lat. (mJ/cm^2)	20	20	25	10	20
Foc. Lat. (µm)	0.8	1.2	1.4	0.4-0.6	0.4-0.6

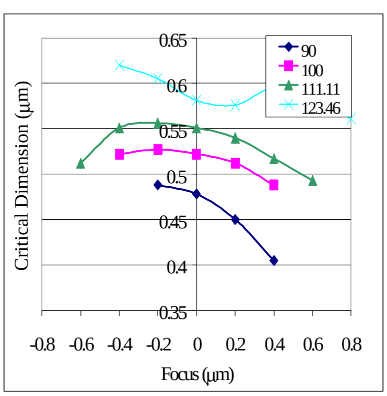

Figure 18: IP3600 (**0.5 µm** /0.26N/ 60 s dev./ No PEB)

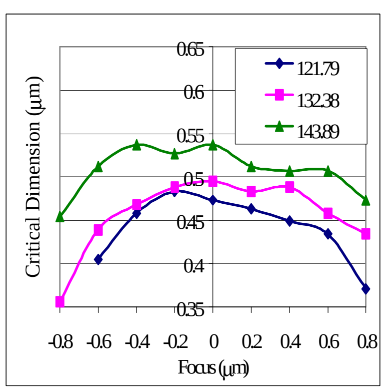

Figure 19: IP3600 (**0.5 µm** /0.20N/ 180 s dev./ PEB)

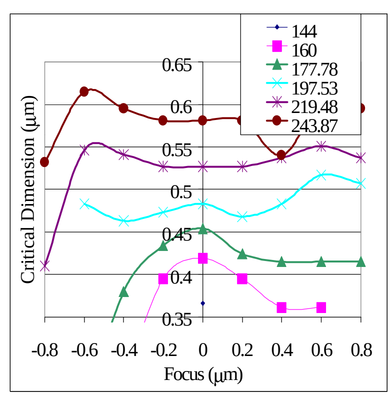

Figure 20: PFI88A5 (**0.5 µm** /0.26N/ 180 s dev./ PEB)

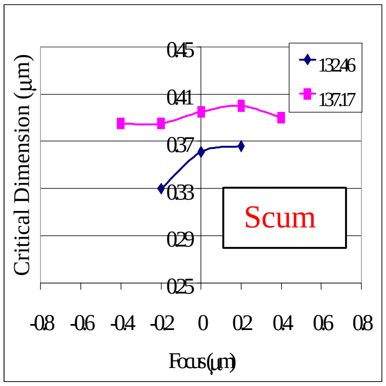

Figure 21: IP3600 (**0.3 µm**/ 0.26N/ 60 s dev./No PEB)

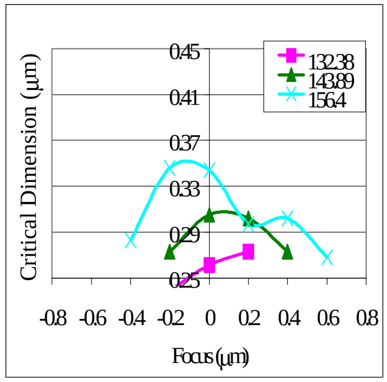

Figure 22: IP3600 (**0.3 µm** / 0.20N/ 180 s dev./ PEB)

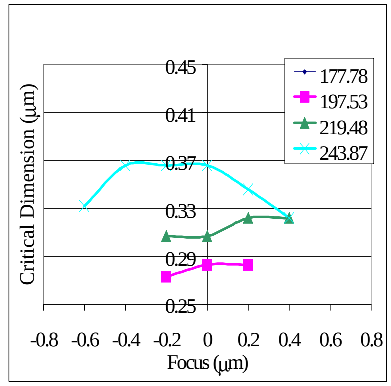

Figure 23: PFI88A5 (**0.3 µm** / 0.26N/ 180 s dev./ PEB)

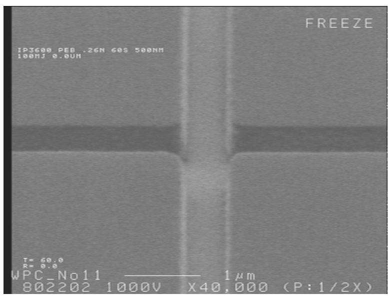

Figure 24: IP3600 (**0.5 µm**/ 0.26N/ 60 s dev./No PEB)

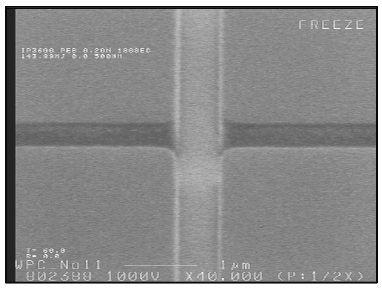

Figure 25: IP3600 (**0.5 µm** / 0.20N/ 180 s dev./ PEB)

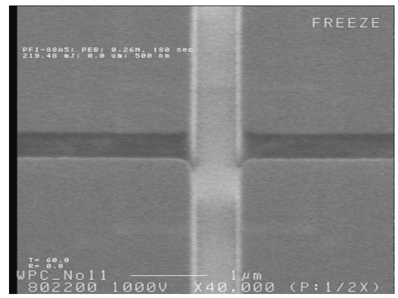

Figure 26: PFI88A5 (**0.5 µm** / 0.26N/ 180 s dev./ PEB)

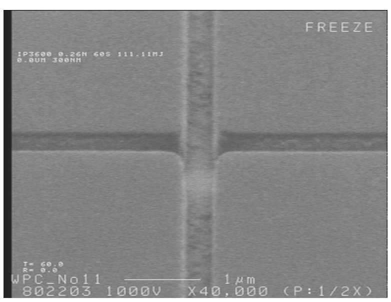

Figure 27: IP3600 (**Scum 0.30 µm** / 0.26N/60 s dev./ No PEB)

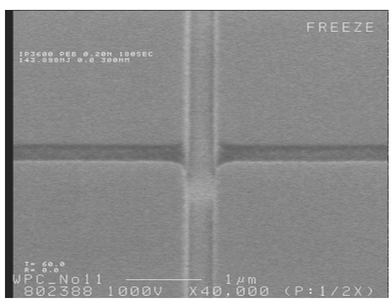

Figure 28: IP3600 (**0.31 µm** / 0.20N/180 s dev./ PEB)

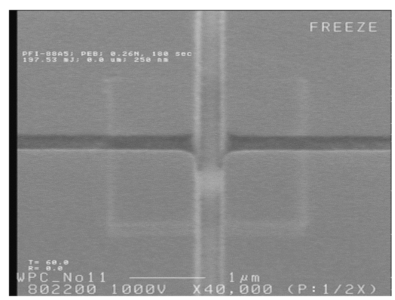

Figure 29: PFI88A5 (**0.25µm** 0.26N/ 180 s dev./ PEB)

4. CONCLUSIONS

Lithography simulation and line-edge optimization have been utilized to improve the process latitude and resolution for I-line optical pattern generators (ALTA 3500). The use of high-resolution resists, high exposure energies, lower developer concentration, long development times and a post-exposure bake improves the process latitude for resist features on photomask substrates. These process improvements lead to better sidewall angles and less CD sensitivity to dose. Manufacturing trials confirmed the process latitude improvements. These changes enable printing with control for resist profiles down to 0.3 µm. The resist profile improvement should reduce the etch bias since there is less need for a descum and breakthrough etch. The use of lower developer concentrations and further bake optimization can potentially lead to further increases in the process window for laser photomask fabrication.

5. ACKNOWLEDGEMENTS

This work was supported by ETEC Systems, Inc. and in part by the SRC/ National Semiconductor Fellowship to B. M. Rathsack. We would like to thank Sumitomo, Clariant, Shipley, Olin and TOK for providing resist samples; FINLE Technologies for PROLITH/2 support and Ron Synowicki at J. A. Woollam for modeling the index of refraction of our photomask substrates.

4. REFERENCES

1. Kuijten, J. P.; Duray, F.; Kinderen T. D., "Analysis of Reticle Contributions to CD Uniformity for 0.25 μm DUV Lithography," *Proc. SPIE-Int. Soc. Eng*. **1998**, *3334*, 620-628.
2. Wong, A. F.; Ferguson, R.A.; Liebmann, L. W.; Mansfield, S. M.; Molless, A. F.; Neisser, M. O., "Lithographic Effects of Mask Critical Dimension Error," *Proc. SPIE-Int. Soc. Eng*. **1998**, *3334*, 106-116.
3. Dammel, R. R.; Sagan, J. P.; Kokinda E.; Eilbeck, N.; Mack, C. A.; Arthur, G. G.; Henderson, C. L.; Scheer, S. A.; Rathsack, B. M.; Willson, C. G., "Improved Simulation of Photoresists using New Development Models," *Proc. SPIE-Int. Soc. Eng*. **1998**, *3333*, 401-416.
4. Yu, J. J.; Meister, C. C.; Vizvary, G.; Xu, C-B.; Fallon, P., "Sub-0.30 μm I-line Photoresist: Formulation Strategy and Lithographic Characterization," *Proc. SPIE-Int. Soc. Eng*. **1998**, *3333*, 1365-1380.
5. Douki, K.; Kajita, T.; Iwanga, S.-I., "Design of I-line Photoresist Capable of Sub-Quarter Micron Lithography; Effects of Novel Phenolic Resin with Controlled End Groups," *Proc. SPIE-Int. Soc. Eng*. **1998**, *3333*, 384 - 392.
6. McAdams, C. L.; Flanagin, L. W.; Henderson, C. L.; Pawloski, A. R.; Tsiartas, P.; Willson, C. G., "The Dissolution of Phenolic Polymers in Aqueous Base: The Influence of Polymer Structure," *Proc. SPIE-Int. Soc. Eng*. **1998**, *3333*, 1171 - 1179.
7. Konnerth, K. L.; Dill, F. H., "IOTA, A New Computer Controlled Thin film Thickness Measurement Tool," *Solid State Electronics* **1972**, *15*, 371-380.
8. Henderson, C. L.; Scheer, S. A.; Tsiartas, P. C.; Rathsack, B. M.; Sagan, J. P.; Dammel, R. R.; Erdmann, A.; Willson, C. G., "Modeling Parameter Extraction for DNQ-novolak Thick Film Resists," *Proc. SPIE-Int. Soc. Eng*. **1998**, *3333*, 256-267.
9. Dill, F. H.; Hornberger, W. P., Hauge; P. S.; Shaw, J.M., "Characterization of Positive Photoresists," *IEEE Trans. Electron Devices* **1975**, *22*(4), 445-452.
10. Erdmann, A.; Henderson, C. L.; Willson, C. G.; Henke, W., "Influence of Optical Nonlinearities of Photoresists on the Photolithographic Process: Basics," *Proc. SPIE-Int. Soc. Eng*. **1997**, *3051*, 529-540.
11. Henderson, C. L.; Pancholi, S. N.; Chowdury, S. A.; Willson, C. G.; Dammel, R. R., "Photoresist Characterization for Lithography Simulation Part 2: Exposure Parameter Measurements," *Proc. SPIE-Int. Soc. Eng*. **1997**, *3049*, 816 - 828.
12. Henderson, C. L.; Tsiartas, P. C.; Pancholi; S. N. Chowdury, S. A.; Dombrowski, K. D.; Willson, C. G.; Dammel, R. R., " Photoresist Characterization for Lithography Simulation Part 3: Development Parameters Measurements," *Proc. SPIE-Int. Soc. Eng*. **1997**, *3049*, 805 - 815.
13. Mack, C. A., *J. Electrochem. Soc.* **1992**, 139, L35.
14. Arthur, G.; Mack, C. A.; Martin, B., "A New Development Model for Lithography Simulation," *Olin Microlithography Seminar, Interface '97* November **1997**, 55-56.
15. Arthur, F.; Wallace, C.; Martin, B., "A Comparison of Recent Development Models in Optical Lithography Simulation," *Proc. SPIE-Int. Soc. Eng*. **1998**, *3332*, 538 - 549.
16. Mack, C. A.; Mueller, K. E.; Gardiner, A. B.; Qin, A.; Dammel, R. R.; Koros, W. J.; Willson, C. Grant, "Diffusivity Measurements in Polymers: I. Lithographic Modeling Results", *Proc. SPIE-Int. Soc. Eng*. **1997**, *3049*, 355-362.
17. Gardiner, A. B.; Qin, A.; Henderson, C. L.; Pancholi, S.; Koros, W. J.; Willson, C. G.; Dammel, R. R.; Mack, C. A.; Hinsberg, W. D., "Diffusivity measurements in polymers: II. Residual Casting Solvent Measurement be Liquid Scintillation Counting", *Proc. SPIE-Int. Soc. Eng.* **1997**, *3049*, 850-860.
18. Kobayashi, H.; Asakawa, K.; Yokoya, Y., "Photomask Blank Enhancement for the Laser Reticle Writer," *Proc. SPIE-Int. Soc. Eng*. **1995**, *2512*, 28 - 44.